Journal of Solid State Chemistry 182 (2009) 2691–2697

Contents lists available at ScienceDirect

Journal of Solid State Chemistry

journal homepage: www.elsevier.com/locate/jssc

Large-scale synthesis, characterization and microwave absorption properties of carbon nanotubes of different helicities

Xiaosi Qi [a], Yi Yang [a], Wei Zhong [a,*], Yu Deng [a], Chaktong Au [b], Youwei Du [a]

[a] Nanjing National Laboratory of Microstructures and Jiangsu Provincial Laboratory for NanoTechnology, Nanjing University, Nanjing 210093, People's Republic of China
[b] Chemistry Department, Hong Kong Baptist University, Hong Kong, People's Republic of China

ARTICLE INFO

Article history:
Received 23 June 2009
Received in revised form
15 July 2009
Accepted 18 July 2009
Available online 25 July 2009

Keywords:
Carbon nanotubes
Complex permittivity
Complex permeability
Reflection loss

ABSTRACT

Carbon nanotubes of high helicity (H-HCNTs, Sample A) have been synthesized in large-scale by pyrolysis of acetylene at 450 °C over Fe nanoparticles derived from coprecipitation/hydrogen reduction method. With controlled introduction of hydrogen during acetylene pyrolysis, CNTs of low helicity (L-HCNTs, Sample B) and worm-like CNTs (Sample C) were obtained in large quantities. The yields of the CNTs products are high, especially that of H-HCNTs (ca. 7474%). The complex permittivity and permeability of Composites A, B, and C that contain Samples A, B and C (30 wt%) were measured in the 2–18 GHz frequency range. Good absorption of electromagnetic wave (reflection loss < -20 dB) was observed in the 7.18–10.68 and 7.5–10.7 GHz range over Composites B and C (2.0–3.0 mm thickness), respectively. Thus, through the suggested route, CNTs can be produced easily and selectively in large quantities. The lightweight materials can be utilized for microwave absorption.

1. Introduction

With the wide-spread use of communication devices, personal computers, local area networks, and radar systems [1–4], electromagnetic interference (EMI) has become a serious problem, especially when microwave of gigahertz is come into consideration. Besides causing severe interruption in systems that are electronically controlled, EMI is potentially harmful to humans. It is known that over exposure to microwave energy can induce abnormal heart beat, weaken immune system, and cause cancer [5–8]. To counteract the ill effects, various kinds of microwave absorption materials (MAMs) that show strong absorption in a wide range of frequency have been synthesized and are on high demand [9–15]. In military industries, MAMs are important as well. Military aircrafts and vehicles with MAMs coating can escape radar detection [16]. It is desirable that the MAMs are mechanically strong but lightweight. Compared with the conventional ferrite materials, soft metallic magnets that have high Snoek's limit and large saturation magnetization (M_S) values are potential MAMs [17]. However, application of this type of materials is restricted because they are heavy, expensive to synthesize, and/or unstable at room temperature. It is hence desirable to fabricate MAMs that are flexible, lightweight, thermally and chemically stable, and show good absorption properties in a wide frequency range. In terms of these criteria, certain carbon materials appear to be good candidates [18–24]. According to computer simulation based on molecular dynamics calculations, helical carbon nanotubes (HCNTs) are unique in electrical, magnetic, and mechanical properties, and are energetically and thermally stable. Potentially, these lightweight materials can be utilized in nanoengineering [25–33]. For example, if an electrical current passed through HCNTs, an inductive magnetic field would be created. The most prominent characteristic of this material is its electromagnetic cross-polarizing ability. Compared to linear CNTs, helical CNTs are more suitable to be used as nano-transformers or nano-switches for microwave absorption [31]. In the past years, the synthesis of HCNTs has been widely studied. Nagy and co-workers reported the generation of HCNTs as by-products in the fabrication of multiwalled CNTs by means of chemical vapor deposition (CVD) [34,35]. Wang et al. reported that HCNTs were formed as by-products in microwave plasma-enhanced CVD (MW-PECVD) synthesis of MWCNTs [36]. However, selective synthesis of HCNTs in large quantities is rare [33,37,38].

Generally speaking, the morphology and quality of HCNTs depend primarily on factors such as carbon source, catalyst nature, reaction temperatures, gas flow rate of reactant, as well as feedstock pressures [39–47]. In this paper, we report the large-scale synthesis of three types of CNTs that contain entrapped Fe nanoparticles by means of acetylene decomposition at 450 °C over Fe catalyst prepared by coprecipitation/reduction method. The helicity of CNTs was controlled by monitoring the rate of hydrogen introduction into the reaction tube. Additionally, the electromagnetic (EM) and microwave absorption properties of the obtained CNTs were investigated in detail.

* Corresponding author. Fax: +86 25 83595535.
E-mail address: wzhong@nju.edu.cn (W. Zhong).

0022-4596/$ - see front matter © 2009 Elsevier Inc. All rights reserved.
doi:10.1016/j.jssc.2009.07.036

2. Experimental

2.1. Synthesis of catalyst precursor

An aqueous solution (59 ml) of $FeCl_2 \cdot 4H_2O$ (0.166 mol) and $FeCl_3 \cdot 6H_2O$ (0.096 mol) were mixed with aqueous NaOH (4 M, 215 ml) at 83 °C, and there was the precipitation of black powder. After about 30 s, a solution of oleic acid (8 ml) dissolved in aqueous NaOH (0.5 M, 220 ml) was added to the mixture with stirring in a span of 20 min. Then aqueous hydrochloric acid ($V_{H_2O} : V_{HCl} = 9$) was added until the pH value was close to 7. The black suspension was filtered out and washed with cycles of distilled water. With the evaporation of water at 80 °C and heating of the black precipitate at 1000 °C in air for 6 h, ferric oxide in red color was obtained.

2.2. Synthesis of CNTs with various helicities

The 0.05 g of the obtained ferric oxide powder was spread on two ceramic plates which were placed symmetrically inside a quartz reaction tube (6 cm inner diameter and 80 cm length, equipped with temperature and gas-flow controls). Subsequently, the ferric oxide powder was in situ reduced in H_2 at 450 °C for 4 h. After the reduction of ferric oxide, acetylene and/or hydrogen was introduced in three different manners into the reaction tube and acetylene decomposition was conducted at 450 °C for 6 h at atmospheric pressure over the reduced Fe nanoparticles. The reaction parameters, types and yields of CNTs products are showed in Table 1. As depicted, the sample (black in color) collected under pure acetylene, C_2H_2+H_2 (5:1) and C_2H_2+H_2 (5:3) are denoted as Samples A, B and C. After cooling to room temperature (RT), 2.651, 0.526, and 0.312 g of Samples A, B and C were collected, respectively, in each ceramic plate.

The samples were examined on an X-ray powder diffractometer (XRD) at RT for phase identification using Cu$K\alpha$ radiation (Model D/Max-RA, Rigaku, Japan). Raman spectroscopic investigations were performed using a Jobin-Yvon Labram HR800 instrument with 514.5 nm Ar^+-laser excitation. Thermoanalysis was carried out using a thermal analysis system (Perkin Elmer TGA7 series) with ca. 5.0 mg of sample heated in air at a rate of 10 °C/min. The morphologies of samples were examined over a transmission electron microscope (TEM) (model JEM-2000EX, Japan) operated at an accelerating voltage of 80 kV and a field-emission scanning electron microscope (FE-SEM model FEI Sirion 200, America) operated at an accelerating voltage of 5 kV. The magnetic properties of the samples were measured at 300 K using a Quantum Design MPMS SQUID magnetometer (Quantum Design MPMS-XL, USA) equipped with a superconducting magnet capable of producing fields of up to 50 kOe. For microwave measurement, the as-prepared CNTs samples were mixed with paraffin (as binder matrix) via ultrasonic agitation to give Composites A, B, and C. Each composite was then pressed into a toroid of 7 mm outer and 3 mm inner diameter. The relative complex permittivity ($\varepsilon_r = \varepsilon_r' - j\varepsilon_r''$) and permeability ($\mu_r = \mu_r' - j\mu_r''$) of the composites were measured in frequency range of 2–18 GHz over an Agilent E8363B vector network analyzer. The tangent of dialect and magnetic loss was calculated as $\tan\delta_E = \varepsilon''/\varepsilon'$ and $\tan\delta_M = \mu''/\mu'$, respectively. The reflection loss (RL) curves were calculated from the relative permittivity and permeability at a given frequency and absorber thickness according to the following equations:

$$Z_{in} = \sqrt{\frac{\mu_r}{\varepsilon_r}}\tanh\left(\frac{j2\pi fd\sqrt{\mu_r\varepsilon_r}}{c}\right) \quad (1)$$

$$RL = 20\log\left|\frac{Z_{in}-1}{Z_{in}+1}\right| \quad (2)$$

where f is frequency of electromagnetic wave, d is the thickness of absorber, c is the velocity of light, and Z_{in} is the input impedance of absorber.

3. Results and discussion

3.1. Characterization and microwave-absorbing properties of Sample A

As shown in Table 1, when only acetylene was introduced into the reaction tube, 2.651 g of Sample A was collected. The yield of carbon species (weight ratio of carbon to iron) is ca. 7474%, and carbon purity (weight ratio of carbon to whole production) 98.59 wt%. As far as we know, such a high yield of HCNTs (Fig. 1) has not been reported before. According to the FESEM and TEM images (Figs. 1a–d), Sample A are made up from V-, Y- and V/Y-shaped entities each with either two or three coiled CNTs connected to a catalyst nanoparticle. The nozzles of the tubes are clearly visible, which are tens of nanometers in wall thickness and 30–70 nm in inner diameter (as indicated by arrows in Fig. 1a). The majority of the HCNTs are coiled in a regular and tight fashion, showing coil pitch and diameters (50–100 nm) smaller and tube length longer than that of HCNTs previously reported [33]. As shown in Table 1, HCNTs of this structure (i.e. Sample A) is also denoted as H-HCNTs (high helicity carbon nanotubes). The selectivity to H-HCNTs is high, up to ca. 93%. The grain size of the entrapped catalyst nanoparticle is ca. 40 nm. It is suggested that the small size of the catalyst nanoparticles obtained by the coprecipitation/reduction method has positive effect on large-scale synthesis of the V- and Y-shaped H-HCNTs. From the XRD pattern of Sample A (not shown here), one can see that the diffraction peaks can be indexed to phases of graphite and Fe_3C, a clear indication of the formation of graphite and Fe_3C during the synthesis of H-HCNTs. There is no XRD signal attributable to α-Fe, implying that the Fe content in Sample A is low.

Fig. 2 shows the EM properties and microwave absorption behavior of Composite A that contains 30 wt% of Sample A. As shown in Fig. 2a, with fluctuations during frequency increase in the range of 2–18 GHz, the real (ε') and imaginary (ε'') part of relative complex permittivity of Composite A declines from 32 to 10 and 18 to 11, respectively. Fig. 2b shows the real (μ') and imaginary (μ'') part of complex permeability obtained over Composite A as a function of frequency. One can see that the former is close to 1.0 while the latter to 0. The low μ' and μ'' values can be related to the low content of Fe_3C in Composite A and the smaller magnetization of ferromagnetic Fe_3C in comparison to

Table 1
Experimental conditions for the preparation of different samples of CNTs.

Sample	Reactant	C_2H_2 flow rate (L/min)	H_2 flow rate (L/min)	Mass of the product (g)	Species as revealed by TEM studies
A	C_2H_2	0.05	0	2.651	H-HCNTs
B	C_2H_2+H_2	0.05	0.01	0.526	L-HCNTs
C	C_2H_2+H_2	0.05	0.03	0.312	Worm-like CNTs

that of α-Fe. According to Eqs. (1) and (2), and using the specific parameters of the composite, the relationship between RL and frequency for Composite A is obtained and shown in Fig. 2c. With increasing thickness of Composite A, the value of RL shifts to lower frequency, suggesting that one can tune the range of absorption frequency by means of adjusting the thickness of composite. It can also be seen that the RL value reaches maximum (−8.25 dB) at 11.8 GHz where composite thickness $d_m = 1.5$ mm. In addition, at $d_m = 1.5$ mm, the bandwidth corresponding to RL values below −5 dB (i.e. over 70% microwave absorption) is about 8.57 GHz. All the values demonstrate that Composite A has good microwave absorption ability even at low H-HCNTs mass fraction (30 wt%).

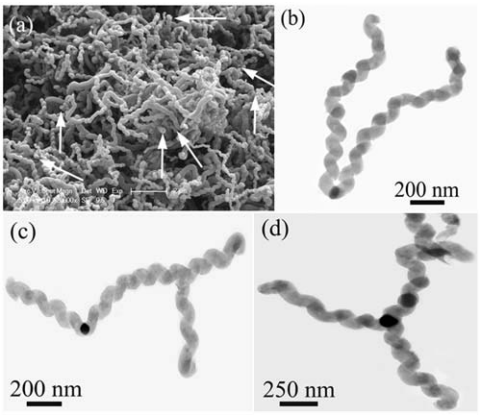

Fig. 1. (a) FESEM images (with arrows indicating nozzles of HCNTs); (b)–(d) TEM images of Sample A.

3.2. Microstructure, microwave EM and microwave-absorbing properties of Sample B

Sample B was fabricated with the introduction of hydrogen into the reaction tube at a low rate. After cooling to RT, 0.526 g of Sample B was collected in each run. The FESEM and TEM images of Sample B are shown in Fig. 3. Compared to Sample A and the HCNTs reported before [31–36], the degree of helicity of Sample B is low (with fewer cycle number, larger coil pitch and shorter tube length). As indicated in Table 1, we also denote Sample B as L-HCNTs (low helicity HCNTs). The L-HCNTs are entities composed of two identical coiled CNTs connected to a catalyst nanoparticle, giving a V-shaped formation. The diameters of the tubes are in the 80–180 nm range. The nozzles of the tubes showing wall thickness of 10 nm and inner diameter of 65–160 nm are clearly visible as indicated by the arrows in Figs. 3a and b. The catalyst nanoparticle (size ca. 60 nm) located at the nodes of the V-shaped entities is wrapped by several layers of carbon. Similar to Sample A, the L-HCNTs are multiwalled and the hollow part of L-HCNTs cannot be observed clearly in the TEM images (Figs. 3c and d).

Unlike that of Sample A, the XRD pattern of Sample B shows a peak ascribable to α-Fe among the Fe_3C peaks (Fig. 4a). The existence of the graphite peak reveals that the L-HCNTs are graphitic. The graphite property of Sample B is confirmed by Raman investigation. The Raman spectrum (Fig. 4b) of Sample B exhibits two peaks, one at 1595.7 cm^{-1} (called G band) and one at 1346.1 cm^{-1} (called D band). One can see that the D band is higher than the G band in intensity and in width. It is known that the G band is due to graphitic layers of high crystallinity, and is corresponding to the E_{2g} mode of graphite (related to C–C vibration of carbon materials with sp^2 orbital structure) [48]. The D band is commonly observed over products obtained in the

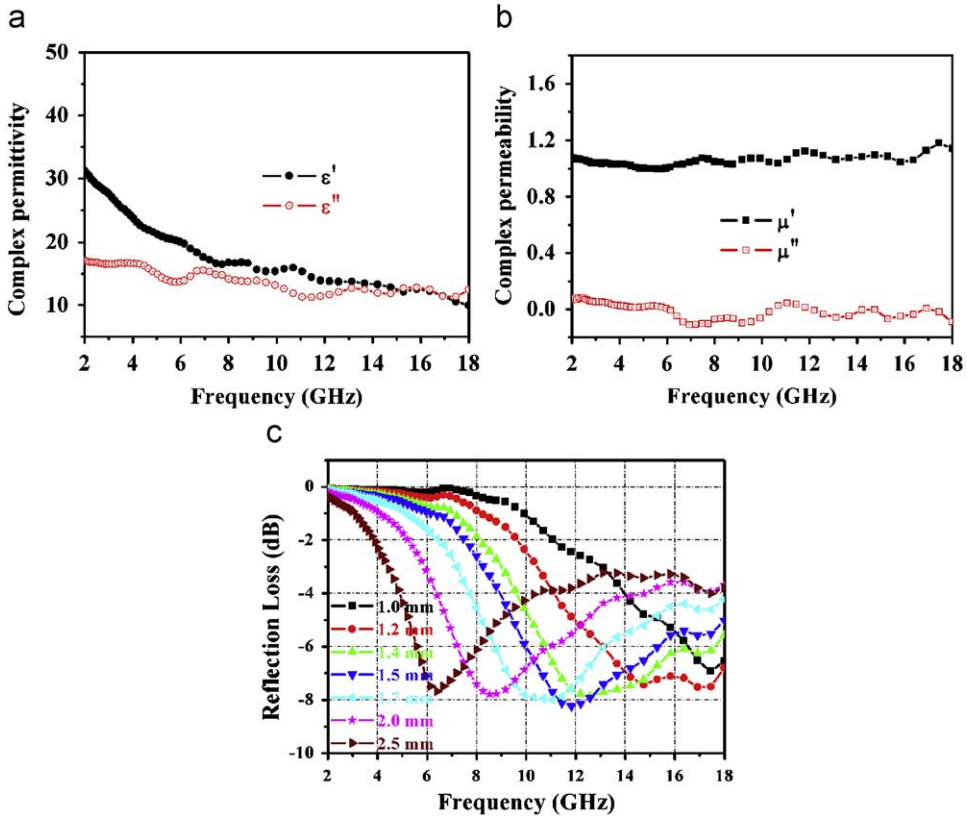

Fig. 2. Microwave measurement of Composite A (containing 30 wt% of Sample A): (a) complex permeability; (b) complex permittivity; and (c) reflection loss versus frequency.

pyrolysis of carbon materials [49]. It is associated with the vibration of carbon atoms with dangling bonds in plane terminations of disordered graphite, and its intensity reflects the amount of lattice defects that are present in the graphite layers.

As shown in Table 1, over 0.05 g of ferric oxide powder (used as catalyst precursor), 0.526 g of Sample B is collected. The corresponding yield of L-HCNTs is ca. 1403%, higher than those of HCNTs reported before [33–47]. The carbon purity of Sample B is high, up to 93.35 wt%. The results are in accord with the result of thermogravimetric (TG) analysis. As shown in Fig. 4c, the 90.5% weight loss confirms the purity of L-HCNTs. The 9.95 wt% remnant can be attributed to ferric oxide powder.

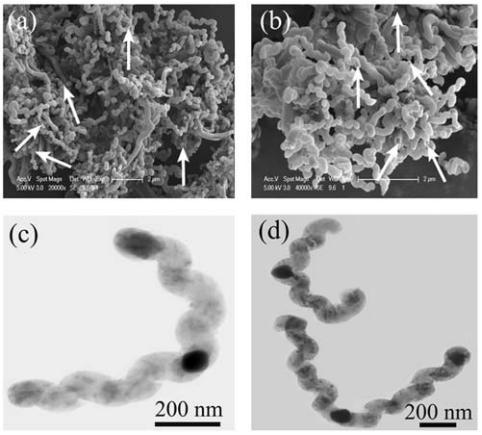

Fig. 3. (a)–(b) FESEM (arrows indicate nozzles); and (c)–(d) TEM images of Sample B.

The EM properties and microwave absorption behavior of Composite B containing 30 wt% of Sample B are shown in Fig. 5. As illustrated in Fig. 5a, Composite B exhibits fluctuation as well as decrease in ε' and ε'' values in the 2–18 GHz frequency range; and the values are smaller than those observed over Composite A (as shown in Fig. 2a). In other words, L-HCNTs shows lower reflection coefficient than H-HCNTs. For microwave absorption, a lower ε' is advantageous in terms of striking a balance between permeability and permittivity. The μ' and μ'' values of Composite B are close to 1.08 and 0, respectively (as shown in Fig. 5b). Compared to Composites A, B shows higher maximum values in both μ' and μ'' (Figs. 2b and 5b). The higher μ' and μ'' values of Composite B are due to the higher magnetization of α-Fe (in comparison to that of Fe_3C) as well as due to the higher α-Fe content in Sample B in comparison to that in Sample A. Fig. 5c shows the plots of dialect tangent and magnetic loss versus frequency. One can see that $\tan\delta_E$ is much higher than $\tan\delta_M$. Because the magnetic parameters are low, we deduce that the RL is mainly due to dielectric loss. The typical relationship between RL and frequency is obtained and shown in Fig. 5d. Compared to the results of Composite A, one can see that there is a shift of maximum reflection point to lower frequency (from 11.8 to 7.18 GHz) in the case of Composite B (Figs. 2c and 5d). It is understandable because in the case of Sample A, much more carbon atoms are trapped in the α-Fe crystalline lattice to form Fe_3C nanoparticles, and hence a higher anisotropy field H_A; similar phenomena have been reported by Liu et al. [50]. The RL value reaches its maximum (−25.78 dB) at 7.18 GHz and at thickness $d_m = 3.0$ mm, while the absorption range below −10 dB is roughly 4–18 GHz. It is worth noting that RL values less than −20 dB can be obtained in the 7.18–10.68 GHz range at composite thickness of 2.0–3.0 mm. A RL value of −20 dB corresponding to 99% of EM wave attenuation can

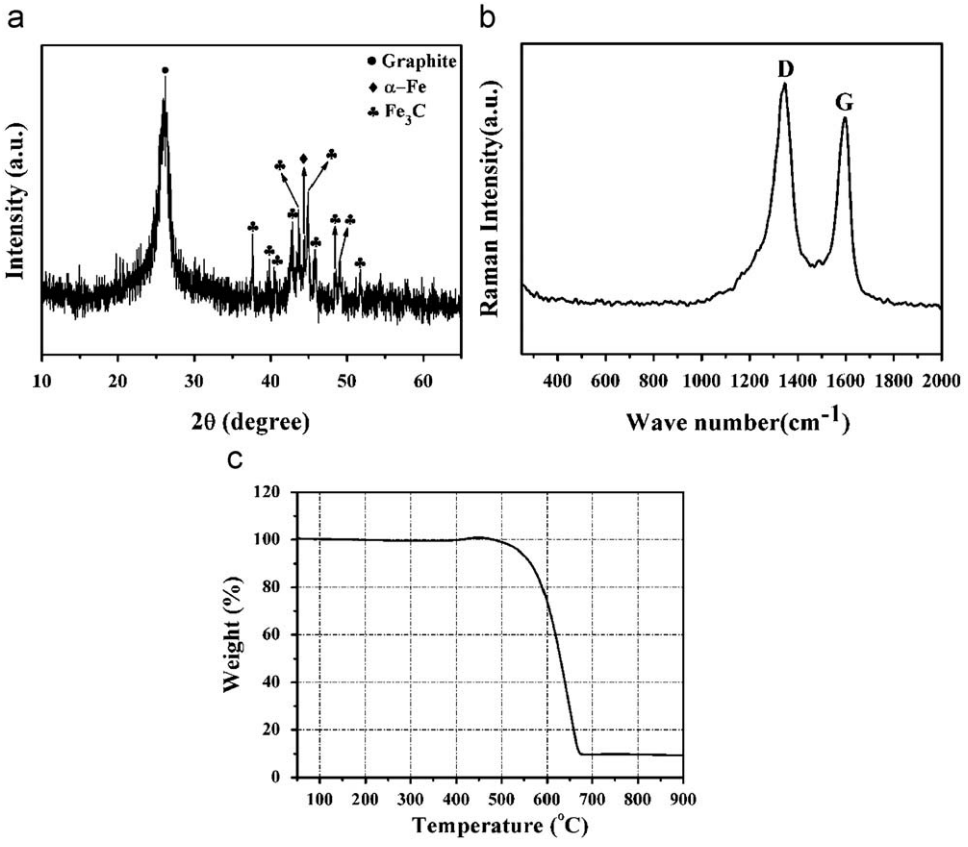

Fig. 4. (a) XRD pattern; (b) Raman spectrum; and (c) TG curve of Sample B.

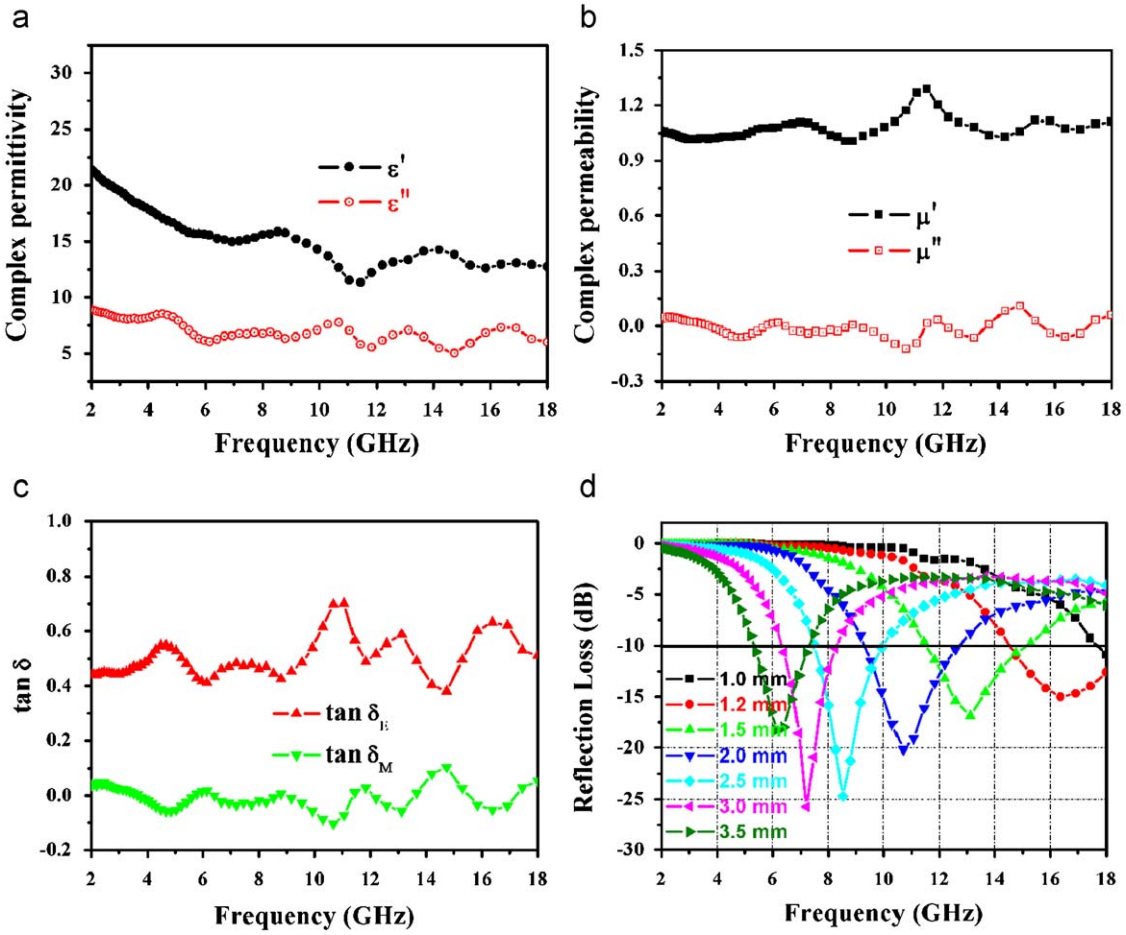

Fig. 5. Microwave measurement of Composite B (containing 30 wt% of Sample B): (a) complex permeability; (b) complex permittivity; (c) loss tangent; and (d) reflection loss versus frequency.

be considered effective in practical applications [3,21,51]. A comparison between Composites A and B shows that the latter exhibits better microwave absorption properties than the former.

3.3. *Effect of flow rate of hydrogen*

At a H_2 flow rate higher than that for the synthesis of Sample B (as shown in Table 1), 0.312 g of Sample C was obtained, and the corresponding yield of carbon species is ca. 891%. The FESEM and TEM images of Sample C are shown in Figs. 6a–d, and one sees worm-like CNTs rather than HCNTs. The selectivity to worm-like CNTs (indicated by arrows in Fig. 6a) is high, around 88%. For each catalyst nanoparticle (ca. 200 nm in size), there are two worm-like CNTs attached to it. Compared to that of Samples A and B, the helicity of the worm-like CNTs can be considered as zero. The size of the catalyst nanoparticles of Sample C is much larger than that of Samples A and B (ca. 40 and 60 nm, respectively). It is clear that the introduction of hydrogen and the rate of hydrogen introduction have an effect on the helicity of CNTs as well as on the size of the entrapped catalyst nanoparticles. As shown in the FESEM and TEM images of Sample C, the sizes of catalyst nanoparticles are similar to the diameters of worm-like CNTs, ranging from 150 to 400 nm. The inner diameter and wall thickness of the worm-like CNTs range from 120 to 350 nm and 30 to 50 nm, respectively. In terms of yield, morphology and helicity of CNTs products, there are distinct variations among Samples A, B, and C. Moreover, compared with Samples A (not shown here) and B (Fig. 4a), Sample C (not shown here) shows higher XRD signals of α-Fe and Fe_3C, revealing that the total amount of α-Fe and Fe_3C in Sample C is larger than that in Sample A or B. With equal weight of catalyst precursor (0.05 g), a higher yield of carbon species would mean a lower total concentration of α-Fe and Fe_3C. The understanding is in consistent with the XRD results of the three samples.

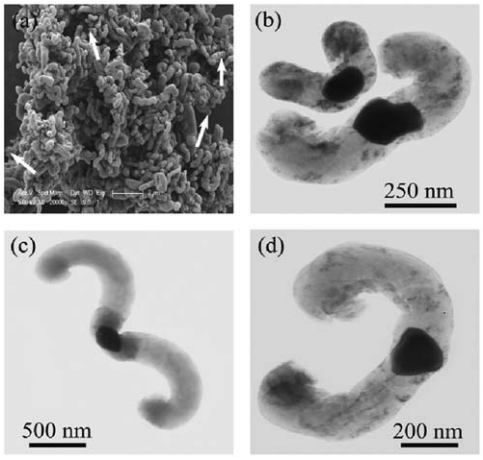

Fig. 6. Typical (a) FESEM image (with tube nozzles indicated by arrows); (b)–(d) TEM images of Sample C.

The EM properties and microwave absorption behavior of Composite C containing 30 wt% Sample C are given in Fig. 7. Similar to the cases of Composites A and B, there is fluctuation and decline (as shown in Fig. 7a) of ε' and ε'' values (from 18 to 10 and 8 to 4, respectively) with increase of frequency. Additionally, the values of ε' and ε'' are lower than those of Composites A and B. The value of μ' and μ'' is close to 1.1 and 0, respectively (Fig. 7b). The μ' of Composite C is slightly higher than that of Composites A and B, plausibly due to the higher content of ferromagnetic Fe nanoparticles in Sample C. The relationship between RL and frequency for Composite C is calculated as before and is shown in Fig. 7c. It can be seen that the samples exhibit good ability of microwave absorption. The maximum RL value (at composite thickness $d_m = 2.8$ mm) reaches -26.39 dB at 7.71 GHz, higher than that of Composite A or B. Also, RL values below -20 dB are obtained in 7.5–10.7 GHz with thickness of Composite C in the 2.0–3.0 mm range. At $d_m = 2.0$ mm, the bandwidth corresponding to RL values below -5 dB is about 10.0 GHz. Clearly, Composite C is superior to Composites A and B in microwave absorption.

It is worth mentioning that due to the nanosize of the three materials, despite the low mass fraction of CNTs (30 wt%) in Composites A, B and C, the materials exhibit good microwave absorption properties. In general, for a mixture of conductor and insulator such as that of CNTs and paraffin, interfacial polarization is an essential contributing factor for dielectric properties due to interfacial charging. In other words, the number of interface in a composite could have an impact on permittivity. On the basis of equal mass fraction of H-HCNTs, L-HCNTs and worm-like CNTs, Composite A should have the highest number of interface while Composite C the lowest because the diameter of H-HCNTs is the smallest while that of worm-like CNTs the biggest among the three materials. This could be the reason why the permittivity of Sample A is largest while that of Sample C the lowest. From another point of view, again on the basis of equal mass fraction, being smaller in size would mean higher in concentration (per unit volume) of a material in a particular matrix. In other words, the concentration of H-HCNTs in Composite A is higher than that of L-HCNTs in Composite B, and that of worm-like CNTs in Composite C. It is envisioned that compared to the cases of Composites B and C, the concentration of Sample A is much closer to the percolation threshold and it is easier to form a conductive network in Composite A. This is reflected by experimental result that ε' of Composite A is bigger than that of Composite B while ε'' of Composite C is the smallest. Moreover, it has been reported that in cases of magnetic nanoparticle/CNT composites, a lower ε' is advantageous in terms of striking a balance between permeability and permittivity. A proper match between dielectric loss and magnetic loss for better penetration of electromagnetic wave would result in enhanced microwave absorption [18,22,23,52]. In our investigations, over equal amount (0.05 g) of catalyst, 2.651, 0.526, and 0.312 g of Samples A, B, and C was collected, respectively. In other words, the concentration of magnetic nanoparticles is the highest in Sample C, and hence the M_S of Sample C should be the highest while that of Sample A the lowest. This perception is confirmed by the magnetization-coercivity curves measured by SQUID at 300 K (not shown). The M_S of

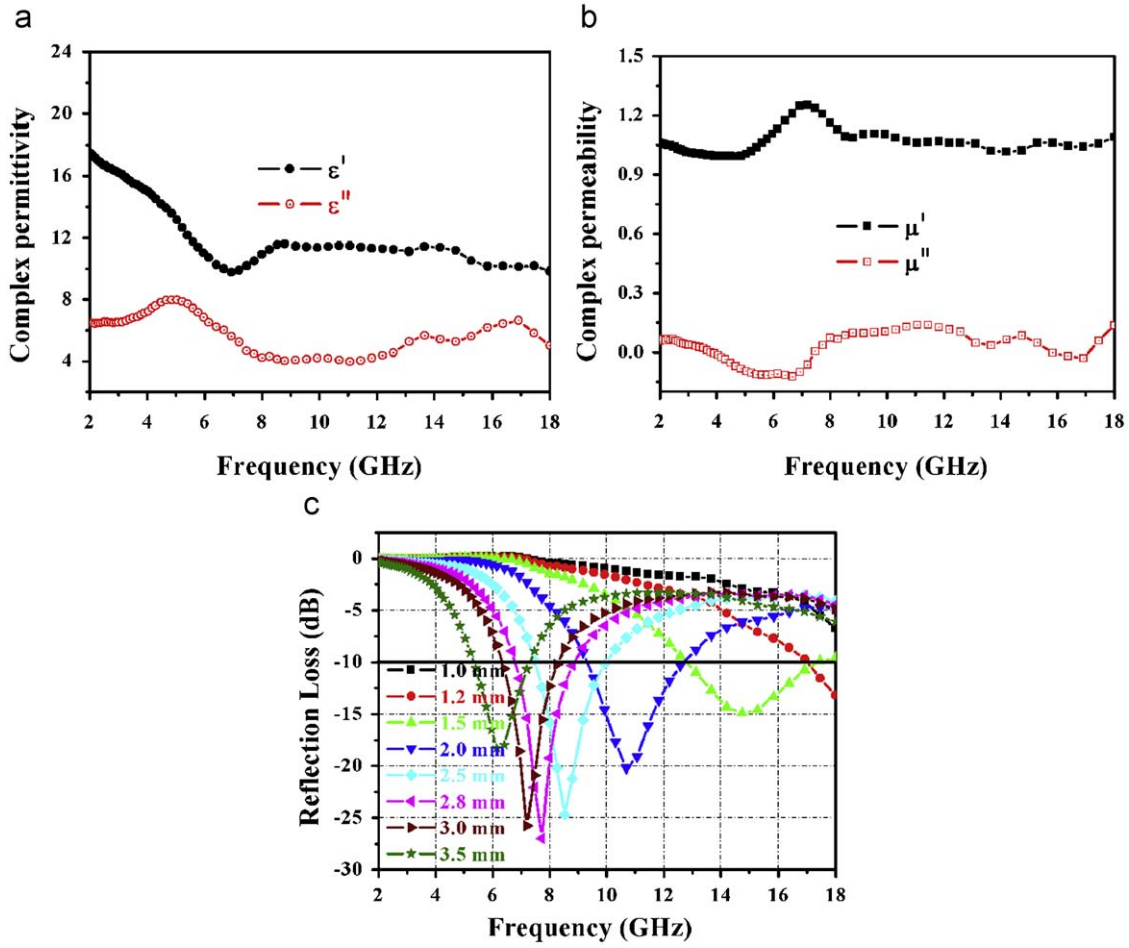

Fig. 7. Microwave measurement of Composite C (containing 30 wt% of Sample C): (a) complex permeability; (b) complex permittivity; and (c) reflection loss versus frequency.

Samples A, B and C are 0.78, 5.11 and 20.56 emu g^{-1}, respectively; and the CNTs with low helicity and length (i.e. L-HCNTs and worm-like CNTs) show a relatively low value of ε' as mentioned above. Thus, the worm-like CNT material is superior to H-HCNTs and L-HCNTs in microwave absorption. Based on the same understanding, the microwave absorbing properties of CNTs can be adjusted by controlling the yield of the material (i.e. concentration of magnetic nanoparticles in the material).

4. Conclusions

We reported a simple and environmentally friendly route for the synthesis of CNTs samples that differ in helicity. H-HCNTs, L-HCNTs and worm-like CNTs were fabricated through the catalytic decomposition of acetylene over catalyst of Fe nanoparticles generated by a combined coprecipitation/hydrogen reduction method. By controlled introduction of hydrogen into the reaction tube, the materials can be produced selectively in high yield. We found that despite the CNTs mass fraction in the composite is low (30 wt%), the materials show good microwave absorbing ability. In the case of Composite C, maximum reflection loss and bandwidth corresponding to reflection loss below −20 dB is −26.39 dB and 3.2 GHz, respectively.

Acknowledgments

This work was supported by the National Natural Science Foundation of China (Grant no. 10674059), the National High Technology Research and Development Program of China (Grant no. 2007AA021805), and the National Key Project for Basic Research (Grant no. 2005CB623605), People's Republic of China.

References

[1] K.M. Lim, M.C. Kim, K.A. Lee, C.G. Park, IEEE Trans. Magn. 39 (2003) 1836–1841.
[2] S. Sugimoto, K. Okayama, S. Kondo, H. Ota, M. Kimura, Y. Yoshida, Mater. Trans. 39 (1998) 1080–1083.
[3] J.R. Liu, M. Itoh, K. Machida, Appl. Phys. Lett. 83 (2003) 4017–4019.
[4] A.N. Yusoff, M.H. Abdullah, S.H. Ahmad, S.F. Jusoh, A.A. Mansor, S.A.A. Hamid, J. Appl. Phys. 92 (2002) 876–882.
[5] A.N. Yusoff, M.H. Abdullah, J. Magn. Magn. Mater. 269 (2004) 271–280.
[6] J.R. Jauchem, K.L. Ryan, M.R. Frei, Bioelectromagnetics 21 (2000) 159–166.
[7] B. Veyret, C. Bouthet, P. Deschaux, R. Deseze, M. Geffard, J. Joussot-Dubien, Bioelectromagnetics 12 (1999) 47–56.
[8] E. Ritcher, T. Berman, E. Ben-Michael, R. Laster, J.B. Westin, Int. J. Occup. Environ. Health 6 (2000) 187–190.
[9] Y.J. Chen, P. Gao, R.X. Wang, C.L. Zhu, L.J. Wang, M.S. Cao, H.B. Jin, J. Phys. Chem. C 113 (2009) 10061–10064.
[10] X.F. Zhang, X.L. Dong, H. Huang, Y.Y. Liu, W.N. Wang, X.G. Zhu, B. Lv, J.P. Lei, Appl. Phys. Lett. 89 (2006) 053115/1.
[11] C.C. Lee, D.H. Chen, Appl. Phys. Lett. 90 (2007) 193102/1.
[12] X.G. Liu, D.Y. Geng, Z.D. Zhang, Appl. Phys. Lett. 92 (2008) 243110/1.
[13] X.G. Liu, D.Y. Geng, H. Meng, P.J. Shang, Z.D. Zhang, Appl. Phys. Lett. 92 (2008) 173117/1.
[14] J.R. Liu, M. Itoh, T. Horikawa, K.I. Machida, J. Appl. Phys. 98 (2005) 054305/1.
[15] Y. Li, C.X. Chen, X.Y. Pan, Y.W. Ni, S. Zhang, J. Huang, D. Chen, Y.F. Zhang, Physica B 404 (2009) 1343–1346.
[16] R.A. Stonier, Sampe J. 27 (1991) 9–17.
[17] V.B. Bregar, IEEE Trans. Magn. 40 (2004) 1679–1684.
[18] X.F. Zhang, X.L. Dong, H. Huang, Y.Y. Liu, W.N. Wang, X.G. Zhu, Appl. Phys. Lett. 89 (2006) 053115/1.
[19] Y.J. Li, C.Z. Zhu, C.M. Wang, J. Phys. D: Appl. Phys. 41 (2008) 125303/1.
[20] X.F. Zhang, X.L. Dong, H. Huang, B. Lv, J.P. Lei, C.J. Choi, J. Phys. D: Appl. Phys. 40 (2007) 5383–5387.
[21] J.R. Liu, M. Itoh, K. Machida, Appl. Phys. Lett. 88 (2006) 062503/1.
[22] R.C. Che, L.M. Peng, X.F. Duan, Q. Chen, X.L. Liang, Adv. Mater. 16 (2004) 401–405.
[23] R.C. Che, C.Y. Zhi, C.Y. Liang, X.G. Zhou, Appl. Phys. Lett. 88 (2006) 033105/1.
[24] A. Wadhawan, D. Garrett, J.M. Perez, Appl. Phys. Lett. 83 (2003) 2683–2685.
[25] S. Ihara, S. Itoh, Carbon 33 (1995) 931–939.
[26] K. Akagi, R. Tamura, M. Tsukada, S. Itoh, S. Ihara, Phys. Rev. Lett. 74 (1995) 2307–2310.
[27] S. Iijima, T. Ichihashi, Y. Ando, Nature 356 (1992) 776–778.
[28] S. Amelinckx, X.B. Zhang, D. Bernaerts, X.F. Zhang, V. Ivanov, J.B. Nagy, Science 265 (1994) 635–639.
[29] P.M. Ajayan, J.M. Nugent, R.W. Siegel, B. Wei, P. Kohler-Redlich, Nature 2000 404 (2000) 243–244.
[30] X.Y. Kong, Z.L. Wang, Nano Lett. 3 (2003) 1625–1631.
[31] W.K. Hsu, M. Terrones, J.P. Hare, H. Terrones, H.W. Kroto, D.R.M. Walton, Chem. Phys. Lett. 262 (1996) 161–166.
[32] A. Volodin, M. Ahlskog, E. Seynaeve, C. Van Haesendonck, A. Fonseca, J.B. Nagy, Phys. Rev. Lett. 84 (2002) 3342–3345.
[33] N.J. Tang, W. Zhong, C.T. Au, A. Gedanken, Y. Yang, Y.W. Du, Adv. Funct. Mater. 17 (2007) 1542–1550.
[34] P. Piedigrosso, Z. Konya, J.F. Colomer, A. Fonseca, G. Van Tendeloo, J.B. Nagy, Phys. Chem. Chem. Phys. 2 (2000) 163–170.
[35] K. Hernadi, A. Fonseca, J.B. Nagy, D. Bernaerts, A.A. Lucas, Carbon 34 (1996) 1249–1257.
[36] X.H. Wang, Z. Hu, Q. Wu, X. Chen, Y. Chen, Thin Solid Films 390 (2001) 130–133.
[37] V. Bajpai, L.M. Dai, T. Ohashi, J. Am. Chem. Soc. 126 (2004) 5070–5071.
[38] H.Q. Hou, Z. Jun, F. Weller, A. Greiner, Chem. Mater. 15 (2003) 3170–3175.
[39] X.H. Zhou, G.L. Cui, L.J. Zhi, S.S. Zhang, New Carbon Mater. 22 (2007) 1–6.
[40] C. Vallés, M. Pérez-Mendoza, P. Castell, M.T. Martínez, W.K. Maser, A.M. Benito, Nanotechnology 17 (2006) 4292–4299.
[41] R.P. Gao, Z.L. Wang, S.S. Fan, J. Phys. Chem. B 104 (2000) 1227–1234.
[42] Y.K. Wen, Z.M. Shen, Carbon 39 (2001) 2369–2374.
[43] M.Z. Wu, L.Z. Yao, G.W. Jiang, W.F. Liu, W.L. Cai, X.G. Li, Z. Yao, J. Inorg. Mater. 18 (2003) 115–120.
[44] J.P. Cheng, X.B. Zhang, J.P. Tu, X.Y. Tao, Y. Ye, F. Liu, Mater. Chem. Phys. 95 (2006) 12–15.
[45] T. Luo, J.W. Liu, L.Y. Chen, S.Y. Zeng, Y.T. Qian, Carbon 43 (2005) 755–759.
[46] J. Liu, S. Webster, D.L. Carroll, Appl. Phys. Lett. 88 (2006) 213119/1.
[47] W. Wang, K.Q. Yang, J. Gaillard, P.R. Bandaru, A.M. Rao, Adv. Mater. 20 (2008) 179–182.
[48] V. Ivanov, A. Fonseca, J.B. Nagy, A. Lucas, P. Lambin, D. Bernaerts, Carbon 33 (1995) 1727–1738.
[49] M.W. Shao, Q. Li, J. Wu, B. Xie, S.Y. Zhang, Y.T. Qian, Carbon 40 (2002) 2961–2963.
[50] J.R. Liu, M. Itoh, T. Horikawa, E. Taguchi, H. Mori, K. Machida, Appl. Phys. A 82 (2006) 509–513.
[51] J.R. Liu, M. Itoh, T. Horikawa, M. Itakura, N. Kuwano, K. Machida, J. Phys. D: Appl. Phys. 37 (2004) 2737–2741.
[52] A. Wadhawan, D. Garrett, J.M. Perez, Appl. Phys. Lett. 83 (2003) 2683–2685.